Three-Dimensional Magnetic Resonance Imaging Bone Models of the Hip Joint Using Deep Learning

Dynamic Simulation of Hip Impingement for Diagnosis of Intra- and Extra-articular Hip Impingement

Guodong Zeng,* PhD, Celia Degonda,[†] MD, Adam Boschung,[†‡] MD,
Florian Schmaranzer,[†‡] MD, PhD, Nicolas Gerber,* PhD, Klaus A. Siebenrock,[†] MD,
Simon D. Steppacher,[†] MD, Moritz Tannast,[†§] MD, and Till D. Lerch,[†‡‖] MD, PhD
Investigation performed at Inselspital, University of Bern, Bern, Switzerland

Background: Dynamic 3-dimensional (3D) simulation of hip impingement enables better understanding of complex hip deformities in young adult patients with femoroacetabular impingement (FAI). Deep learning algorithms may improve magnetic resonance imaging (MRI) segmentation.

Purpose: (1) To evaluate the accuracy of 3D models created using convolutional neural networks (CNNs) for fully automatic MRI bone segmentation of the hip joint, (2) to correlate hip range of motion (ROM) between manual and automatic segmentation, and (3) to compare location of hip impingement in 3D models created using automatic bone segmentation in patients with FAI.

Study Design: Cohort study (diagnosis); Level of evidence, 3.

Methods: The authors retrospectively reviewed 31 hip MRI scans from 26 symptomatic patients (mean age, 27 years) with hip pain due to FAI. All patients had matched computed tomography (CT) and MRI scans of the pelvis and the knee. CT- and MRI-based osseous 3D models of the hip joint of the same patients were compared (MRI: T1 volumetric interpolated breath-hold examination high-resolution sequence; 0.8 mm^3 isovoxel). CNNs were used to develop fully automatic bone segmentation of the hip joint, and the 3D models created using this method were compared with manual segmentation of CT- and MRI-based 3D models. Impingement-free ROM and location of hip impingement were calculated using previously validated collision detection software.

Results: The difference between the CT- and MRI-based 3D models was <1 mm, and the difference between fully automatic and manual segmentation of MRI-based 3D models was <1 mm. The correlation of automatic and manual MRI-based 3D models was excellent and significant for impingement-free ROM ($r = 0.995$; $P < .001$), flexion ($r = 0.953$; $P < .001$), and internal rotation at 90° of flexion ($r = 0.982$; $P < .001$). The correlation for impingement-free flexion between automatic MRI-based 3D models and CT-based 3D models was 0.953 ($P < .001$). The location of impingement was not significantly different between manual and automatic segmentation of MRI-based 3D models, and the location of extra-articular hip impingement was not different between CT- and MRI-based 3D models.

Conclusion: CNN can potentially be used in clinical practice to provide rapid and accurate 3D MRI hip joint models for young patients. The created models can be used for simulation of impingement during diagnosis of intra- and extra-articular hip impingement to enable radiation-free and patient-specific surgical planning for hip arthroscopy and open hip preservation surgery.

Keywords: FAI; hip impingement; MRI; CT; impingement simulation

Femoroacetabular impingement (FAI) is a major cause of hip pain and osteoarthritis in young adult patients of childbearing age[8] that is most often symptomatic during sports.

FAI often limits range of motion (ROM) and has been defined by a painful early osseous abutment between the femoral head–neck junction and the acetabular rim.[8,31,44] Usually patients have pain during sports, squats, or other dynamic activities of daily living.[8,31,44] Although FAI has been described as a dynamic osseous conflict, actual 2-dimensional standard imaging is static and cannot
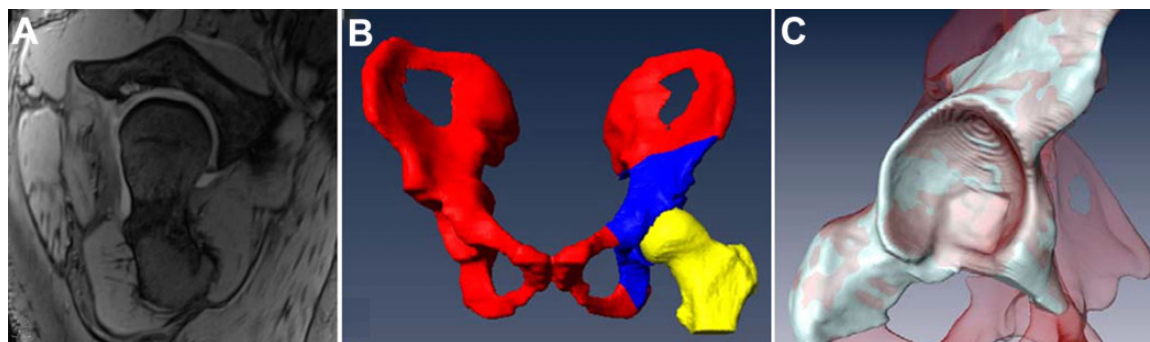
Figure 1. (A) The high-resolution unilateral 3D MRI scan of the T1 volumetric interpolated breath-hold examination sequence and (B) the MRI-based 3D model are shown. (C) An acetabular MRI-based 3D model (white) and a CT-based 3D model (red transparent) are shown to calculate accuracy.

visualize the location of impingement during these painful activities. In addition, differentiation between intra- and extra-articular FAI remains a challenge during clinical examination[30] because many clinical tests have low specificity.[29] Extra-articular hip impingement can be located anteriorly[17] (subspine FAI) or posteriorly[24] (ischiofemoral FAI) and is associated with abnormalities of femoral version (FV). Theoretically, abnormal FV[22,33] may compensate for or contribute to the impingement conflict and can cause extra-articular FAI.[17,20] So far, the exact effect of FV for patients undergoing surgical treatment remains controversial.[7,16]

Surgical planning of FAI surgery was limited by the inability to assess the dynamic location of impingement. To overcome these problems, dynamic 3-dimensional (3D) impingement simulation to calculate impingement-free ROM using computed tomography (CT)–based osseous 3D models was developed.[42] It allows simulation of human hip ROM and can reproduce painful and patient-specific movements of patients with symptomatic FAI and complex hip deformities.[35,39] Because of the considerable radiation exposure of CT scans,[48] this 3D impingement simulation is not used routinely for patients with symptomatic FAI. For these patients of young age, manual segmentation of magnetic resonance (MR) imaging (MRI)–based osseous 3D models of the hip joint represents a noninvasive and radiation-free alternative.[18] This simulation can provide a patient-specific and circumferential analysis of the deformity. Using this simulation, we can calculate impingement-free ROM in hips with severe deformities,[35] including hips with severe cam deformities and

Legg-Calvé-Perthes disease.[39] Analyzing the 3D morphology has implications for planning of FAI surgery.[36]

Mainly because of the time-consuming nature of manual segmentation, 3D MRI bone models have not been applied routinely. In the current study, a novel MRI sequence was added to the MRI, and convolutional neural networks (CNNs) were used to develop fully automatic bone segmentation for T1 volumetric interpolated breath-hold examination (VIBE) 3D MRI scans of the hip joint (Figure 1). In deep learning, or machine learning, a CNN is a type of artificial neural network that is used for image processing, classification, and segmentation. We then used the created MRI models for impingement simulations (Video Supplement 1) and compared them with matched CT-based 3D models of the same patients (Video Supplement 2).

The primary purpose of this study was to evaluate the accuracy of the MRI models created using the CNN method. Additional aims were to correlate range of hip motion of manual and automatic segmentation and to compare the location of intra- and extra-articular impingement on the 3D models created using this method in patients of young age with symptomatic FAI.

METHODS

We performed an institutional review board–approved retrospective and comparative study including a total of 31 hips of 26 symptomatic patients with a mean age of 27 ± 7 years. All patients exhibited anterior hip pain and a positive anterior impingement test at the time of image
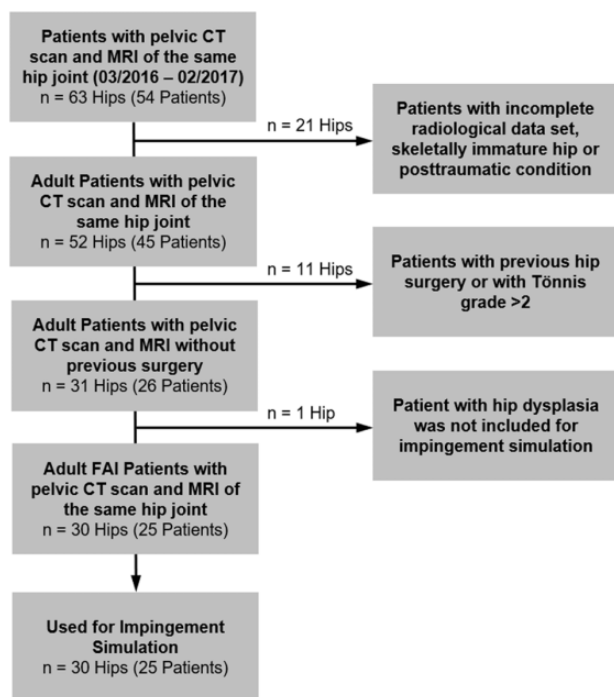
Figure 2. Flowchart showing the inclusion and exclusion criteria of the patient series. FAI, femoroacetabular impingement.

acquisition. We evaluated hip MRI scans of symptomatic patients consecutively who had been referred to our center (Inselspital Bern, University of Bern, Switzerland) for hip preservation surgery in a 1-year period (March 2016–February 2017). Informed consent was obtained from all patients.

Inclusion and Exclusion Criteria

Inclusion criteria were the following: symptomatic patients with hip pain; standard anteroposterior (AP) radiographs; radiographic signs of skeletal maturity; and availability of both standardized pelvic CT scans and direct MR arthrography of the same hip, including the entire pelvis and distal femoral condyles. We retrospectively reviewed our institutional imaging database for all patients for whom direct MR arthrography and a 3D CT scan of the pelvis and knee were performed between March 2016 and February 2017. A total of 63 hips underwent both an MRI scan and a CT scan; of these, we excluded 32 hips because of incomplete radiological data set, skeletally immature hips, previous hip surgery, and posttraumatic conditions. The remaining 31 adult hips were evaluated for accuracy of the 3D bone model in the final study cohort (Figure 2); all participants were part of a previous study by us.[18] For impingement simulation, 30 hips with FAI were evaluated. One patient with hip dysplasia was not included for impingement simulation (Figure 2).

The characteristics and radiological data of the patients are shown in Table 1. Patients had a mean age of 27 years,

TABLE 1
Characteristics and Radiological Data of the Study Group
(N = 31 Hips in 26 Patients)[a]

Parameter	Value
Age, y	27 ± 7 (17 to 41)
Sex, % male	48
Side, % right	61
Bilateral hips, %	16
Height, cm	176 ± 6 (163 to 186)
Weight, kg	83 ± 20 (49 to 117)
Body mass index	27 ± 6 (18 to 38)
LCE angle, deg	31 ± 10 (12 to 56)
Acetabular index, deg	4 ± 8 (−15 to 20)
Extrusion index, %	20 ± 8 (1 to 36)
Alpha angle, deg	51 ± 11 (35 to 84)
FV, deg	25 ± 12 (7 to 54)
Acetabular version, deg	18 ± 6 (7 to 31)
Hip abnormalities, No. of hips (%)[b]	
Cam-type FAI	7 (23)
Pincer-type FAI	5 (16)
Mixed-type FAI	3 (10)
Developmental dysplasia	1 (3)[c]
Increased FV	7 (23)
Cam-type FAI with decreased FV	5 (16)

[a]Data are expressed as mean ± SD (range) unless otherwise indicated. FAI, femoroacetabular impingement; FV, femoral version; LCE, lateral center-edge.

[b]Definitions were based on previously published reference values: cam-type FAI = alpha angle >60°[37]; pincer-type FAI[26] = LCE angle >40°[40]; mixed-type FAI = combination of cam- and pincer-type FAI[45]; developmental dysplasia = LCE angle <22°[40]; increased FV = FV >25°[22]; decreased FV = FV <10°[22].

[c]This patient was included for analysis of accuracy and was excluded for impingement simulation.

and 48% were male. All included patients were symptomatic at the time of image acquisition. For evaluation of accuracy of the 3D models, 31 hips were used. For impingement simulation 30 hips were used. Two patients had avascular necrosis of the femoral head.

Clinical Evaluation and Examination

The patients were examined clinically in the outpatient clinic for hip surgery by one of our attending hip surgeons (M.T. and K.A.S.) with experience in hip preservation surgery. Preoperative planning was the reason to perform a CT scan in addition to MRI in patients with inconclusive clinical and radiographic findings and suspected extra-articular hip impingement.

The routine clinical examination included a thorough acquisition of the patient history, a goniometric measurement of the hip ROM, and anterior and posterior impingement tests.[44] The anterior impingement test was performed routinely with the patient in the supine position and was considered positive if the patient exhibited pain at 90° of flexion and forced internal rotation[44] (IR) combined with adduction. The posterior impingement test (apprehension test) was performed with the patient in the supine position with hyperextension of the hip. It was considered positive if
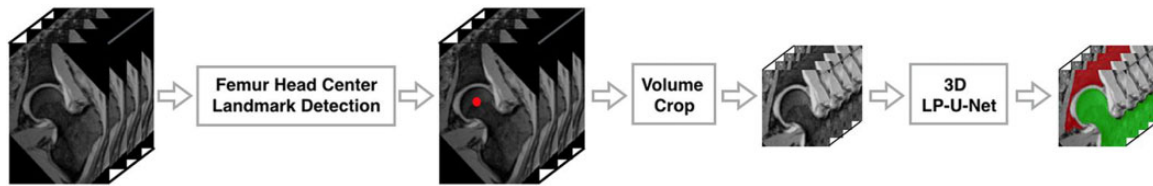
Figure 3. The workflow for automatic segmentation of MRI-based 3D models.

the patient exhibited pain with forced external rotation (ER).[44]

Radiographic Examination

AP pelvic radiographs were obtained routinely for diagnostic preoperative evaluation that was performed in a standardized manner[44] with the patient in the supine position. One observer (T.D.L.) assessed radiographic parameters (Table 1) to describe the femoral and acetabular morphology on AP pelvic radiographs using previously validated software (Hip2Norm; University of Bern).[43,50] Radiographic diagnosis of cam- and pincer-type FAI was based on previously published reference values on conventional AP pelvic radiographs.[40]

Operative Procedures

Of the 31 hips, 19 were treated surgically. Procedures included open hip surgery and hip arthroscopy for cam resection and femoral derotation osteotomy. Total hip arthroplasty was performed for 2 hips with avascular necrosis of the femoral head.

Imaging Technique

MR arthrography was performed according to a standardized protocol on a 3-T scanner (Siemens Medical Solutions). MRI was performed using large flexible surface coils after fluoroscopy-guided intra-articular injection of saline-diluted gadolinium-DTPA (diethylenetriamine penta-acetic acid; Dotarem 1:200; Guerbert AG) was performed. In addition to the previously described routine protocol,[18] we used a unilateral high-resolution T1 VIBE sequence for segmentation of 3D models of the hip. For positioning of landmarks, a bilateral 3D sequence of the pelvis and a bilateral 3D sequence of the knee were used (Figure 1A). The field of view (FOV) of the high-resolution unilateral 3D sequence of the hip covered the proximal femur and the unilateral acetabulum (Figure 1A). The FOV of the bilateral 3D sequence covered the entire pelvis (Figure 1A), and the FOV of the knee joint covered the included bilateral distal femur.

The following 3D MR sequences[18] were obtained: (1) an axial-oblique 3D VIBE for the symptomatic unilateral hip joint to provide high-resolution data (repetition time [TR]/echo time [TE], 15/3.3 milliseconds; flip angles, 4° and 24°; slice thickness, 0.78 mm; FOV, 160 × 160 mm; matrix size, 192 × 192 mm; isotropic voxel size, 0.78 mm³, acquisition time [AT], 9 minutes for 128 slices) (Figure 1A); (2) a T1

VIBE Dixon including the entire pelvis (TR/TE1/TE2, 3.94/1.27/2.5 milliseconds; flip angle, 9°; slice thickness, 1 mm; FOV, 312 × 400 mm; matrix size, 175 × 320 mm; anisotropic voxel size, 1.2 × 1.2 × 1 mm) acquisition time was 32 seconds for 192 slices; and (3) a second T1 VIBE Dixon (same parameters) for the knee. The total AT was 32 minutes for the entire MR examination. For some patients, leg traction was performed according to a previously described technique.[32,34]

Pelvic CT scan was performed using 1-mm slice thickness (Somatom Definition Flash/Edge; Siemens Medical Solutions) as described in a previous study.[39] The scanned volume of the pelvis included the bilateral hip joints (voltage, 120 kVp; intensity, 300 mAs; pitch, 0.8; FOV, 50 cm; voxel size, 1 mm³; convolution kernel, I31f) and the knee, including the bilateral distal femur (same parameters). The radiation dose of the pelvic CT scan was the following: the mean dose-length product of the patient series was 295 ± 124 mGy·cm (range, 138-713 mGy·cm).

Manual Bone Segmentation

Manual segmentation of MRI- and CT-based osseous 3D models was performed previously and by 2 different observers (C.D. and T.D.L.). This resulted in a total number of 62 3D models of 31 hip joints. Based on axial CT scan, threshold-based segmentation of a 3D surface of the pelvis and the femur was performed semiautomatically using commercial software (Amira Visualization Toolkit; Visage Imaging Inc). Based on high-resolution MRI scans (axial-oblique T1 VIBE) of the unilateral hip, manual segmentation of MRI-based 3D models (Figure 1C) was performed. The manual segmentation was performed individually using the same software by 2 different observers (C.D. and T.D.L.) and lasted up to 4 hours for each hip joint. In addition, we performed 30 manual segmentations of MRI-based 3D models for training, which are not included in the current study.

Automatic Bone Segmentation

A deep learning–based, fully automatic method for 3D hip joint segmentation from MRI scans was developed by one of the authors (G.Z.). The method used (Figure 3) consisted of 2 stages. The first stage included detection of the femoral head center (FHC) using a landmark detection network. The detected FHC allowed cropping of the original data set, including the joint space, the femoral head, and the acetabulum. The second stage included another neural network that was trained to segment the cropped hip joint data. The

TABLE 2
Accuracy of the Fully Automatic MRI-Based 3D Models
Versus Manual MRI-Based 3D Models[a]

Parameter[b]	Acetabular Models	Femoral Models
Dice coefficient	97 ± 2 (92-99)	98 ± 1 (93-99)
Precision	96 ± 3 (89-99)	98 ± 2 (92-100)
Recall	97 ± 2 (89-100)	97 ± 3 (87-100)
Average surface distance, mm	0.3 ± 0.5 (0.1-3)	0.2 ± 0.1 (0.1-0.5)
Maximum, mm (also called Hausdorff distance)	9.7 ± 8 (3-39)	5.7 ± 2 (2-13)

[a]Data are expressed as mean ± SD (range). 3D, 3-dimensional; MRI, magnetic resonance imaging.
[b]Terms are explained in the Supplemental Material.

TABLE 3
Accuracy of the Manual MRI-Based 3D Models
Versus CT-Based 3D Models[a]

Parameter, mm[b]	Acetabular Models	Femoral Models	Absolute Difference
Average surface distance	0.9 ± 0.2 (1-2)	0.7 ± 0.1 (0-1)	0.2 ± 0.2 (0-1)
Deviation	1.6 ± 0.3 (1-3)	1.4 ± 0.2 (1-2)	0.3 ± 0.2 (0-1)
Root Mean Square	1.8 ± 0.4 (1-3)	1.5 ± 0.2 (1-2)	0.3 ± 0.3 (0-1)

[a]Data are expressed as mean ± SD (range). 3D, 3-dimensional; CT, computed tomography; MRI, magnetic resonance imaging.
[b]Terms are explained in the Supplemental Material.

hip joint segmentation network was based on the LP-U-net, which was introduced in a previous study.[49] In this network, holistic decomposition convolution and dense upsampling convolution were applied at the beginning and end of the 3D U-net, respectively. LP-U-net can reduce the graphics card (graphics processing unit) memory for subsequential processing while incorporating larger context information for a better performance. Automatic segmentation of 1 hip joint was performed in 1 to 5 minutes.

CNNs were used to develop fully automatic bone segmentation of the hip joint for T1 VIBE images. A standard 3-fold cross-validation study was conducted using the 3D axial-oblique T1 VIBE MRI scans of the unilateral hip joint of the 31 hips (see the Supplemental Material for this article). Specifically, the 31 data were randomly split into 3 groups. Each time, 1 group (10 hips) was used as testing data, and the remaining 2 groups were used as training data. This process was repeated 3 times in order that each group was used once as testing data. We used the Dice similarity coefficient (DSC) and average surface distance (ASD) to evaluate accuracy. Our method was implemented via Python using the TensorFlow framework. Segmentation was performed on a workstation with a 3.6-GHz Intel i7 central processing unit (CPU, Intel Corp) and a GTX 1080 Ti graphics card with 11 GB of graphics processing unit memory.

Outcome Parameters

We used CNN for fully automatic MRI bone segmentation of the hip joint and compared it with manual segmentation of 3D models of the hip joint of the same patients to evaluate the accuracy of 3D models created using this method. We used patient-specific hip impingement simulation for evaluation of impingement-free ROM and location of hip impingement.

The manual and automatic segmentation methods were assessed according to the following 3 outcomes: (1) accuracy of the 3D models, (2) impingement-free ROM of the hip joint, and (3) location of impingement. Accuracy was determined using the same commercial software (Amira) that was used for manual segmentation. The MRI-based and CT-based models of the same hip joint were compared in

this software using the transform editor to align 2 surfaces (Figure 1C). After alignment, the surface distance between two 3D models was calculated, with the CT-based model serving as the gold standard.

Dynamic Simulation of Hip Impingement

Specific software was used to assess impingement-free ROM and location of hip impingement. The software is based on a validated collision detection algorithm.[27] The following ROM parameters were calculated in 1° increments: flexion, extension, IR and ER in extension, abduction, adduction, and IR and ER at 90° of flexion. The inter- and intraobserver correlation coefficient was large for ROM values (of impingement simulation) in a previous publication.[18] In addition, we evaluated 2 clinically important motion patterns with combined hip movements. The first motion pattern is the anterior impingement test,[44] also called the flexion-adduction–IR test.[3] Furthermore, with the second motion pattern, we aimed for simulation of the posterior impingement test (apprehension test).

The location of impingement was assessed using a clock-face system for the femur and the acetabulum separately, similar to previous publications.[17] Intra- and extra-articular hip impingement were assessed separately. Extra-articular hip impingement was analyzed anteriorly (subspine) and posteriorly (ischiofemoral). The software uses a validated medical research framework and was described in a previous publication.[27]

Statistical Analysis

Statistical analysis was performed using 2 software programs. Winstat software (R. Fitch Software) was used to test for normal distribution using the Kolmogorov-Smirnov test for continuous variables. The Pearson correlation coefficient was used because the variables were normally distributed. Absolute mean differences were calculated for continuous ROM variables. To compare the location of impingement between CT- and MRI-based models, the chi-square test was used for the 12-clock positions of the femur and the acetabulum independently. Bland-Altman
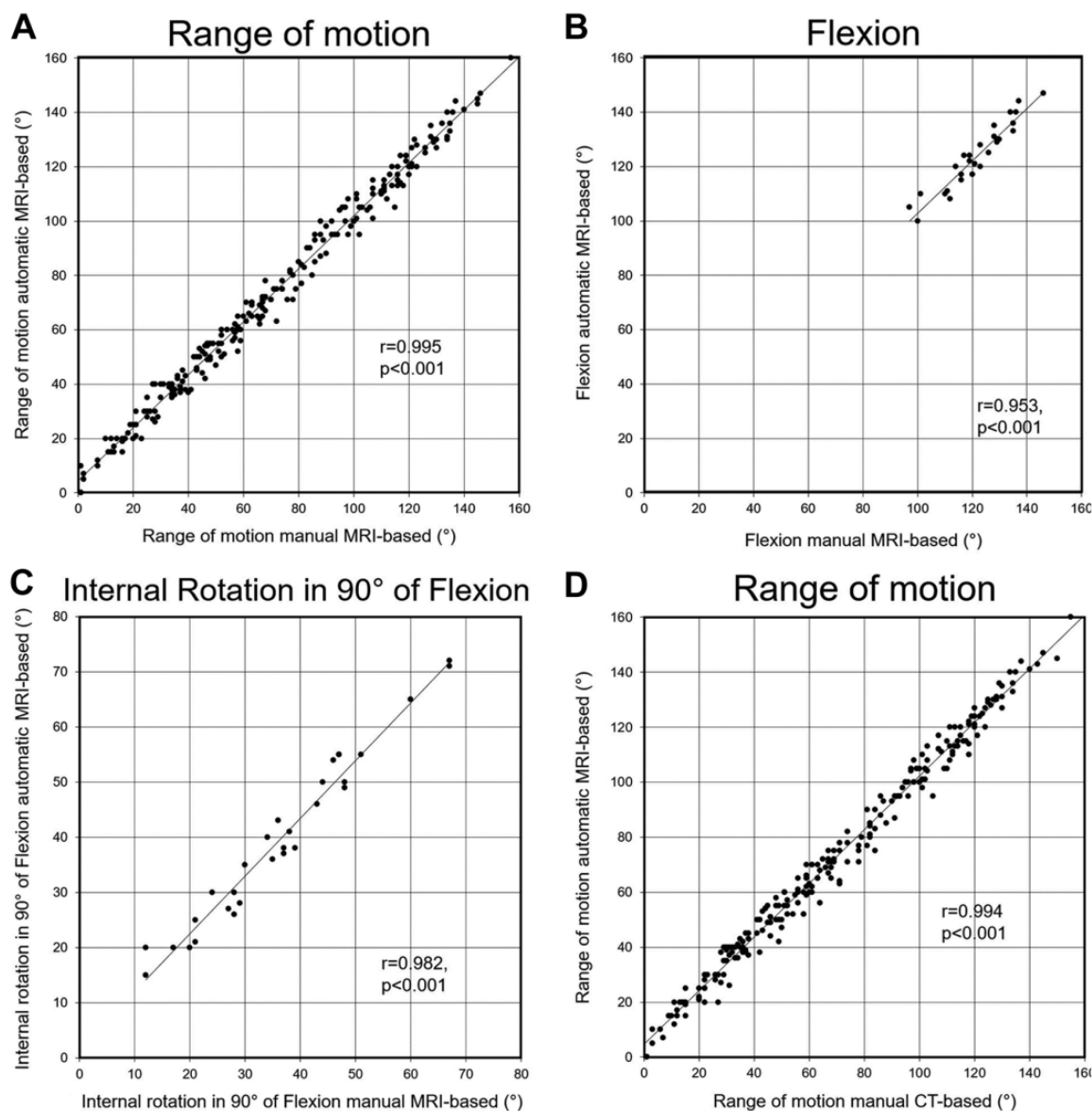
Figure 4. The correlation between automatic and manual MRI-based 3D models for (A) all range of motion (ROM) values, (B) flexion, and (C) internal rotation at 90° of flexion and (D) the correlation between CT-based and manual MRI-based 3D models for all ROM values.

analysis was performed to search for a systematic error using Medcalc software (Version 17.6).

RESULTS

Accuracy of the 3D Models

The CNN model achieved a DSC of 97% for the acetabulum and 98% for the femur (Table 2). The difference between the automatic and manual MRI-based 3D models was <1 mm, and the ASD was 0.3 ± 0.5 mm for the proximal femur and 0.2 ± 0.1 mm for the acetabulum (Table 2). The difference

between the CT-based and manual MRI-based 3D models was <1 mm (Table 3).

Impingement-Free ROM of the Hip Joint

The correlation between automatic and manual MRI-based 3D models was excellent and significant for impingement-free ROM ($r = 0.995$; $P < .001$) (Figure 4A) and for flexion ($r = 0.953$; $P < .001$) and IR at 90° of flexion ($r = 0.982$; $P < .001$) (Table 4 and Figure 4, B and C). The absolute difference was <6° for all parameters (Table 4), and the absolute difference was <4° for flexion (3.0°) and IR at 90° of flexion (3.6°) (Table 4).

TABLE 4
Results of the Range of Motion Values Comparing Manual and Automatic MRI-Based 3D Models Using Specific Software[a]

Parameter, deg	Manual MRI-Based 3D Models	Automatic MRI-Based 3D Models	Absolute Difference, Manual vs Automatic MRI	Correlation Coefficient, Manual vs Automatic MRI
Flexion	122 ± 11 (97 to 146)	124 ± 12 (100 to 147)	3.0 ± 2.8 (0 to 9)	0.953
Extension	60 ± 31 (1 to 100)	63 ± 30 (0 to 100)	4.1 ± 2.7 (0 to 9)	0.989
Internal rotation in extension	114 ± 25 (83 to 172)	115 ± 21 (87 to 162)	4.2 ± 3.2 (0 to 12)	0.981
External rotation in extension	42 ± 22 (–4 to 81)	45 ± 21 (0 to 84)	3.1 ± 2.4 (0 to 9)	0.989
Abduction	62 ± 14 (20 to 81)	64 ± 14 (25 to 85)	3.6 ± 2.3 (0 to 10)	0.969
Adduction	28 ± 15 (1 to 56)	34 ± 15 (0 to 60)	5.8 ± 2.9 (1 to 13)	0.971
Internal rotation at 90° of flexion	38 ± 16 (12 to 73)	40 ± 16 (15 to 72)	3.6 ± 2.7 (0 to 8)	0.982
External rotation at 90° of flexion	100 ± 22 (28 to 126)	101 ± 21 (40 to 130)	4.2 ± 3.2 (0 to 12)	0.974

[a]Data are expressed as mean ± SD (range). 3D, 3-dimensional; MRI, magnetic resonance imaging.

TABLE 5
Results of Automatic MRI-Based and CT-Based Calculations of Range of Motion Using Specific Software[a]

Parameter, deg	Manual CT-Based 3D Models	Automatic MRI-Based 3D Models	Absolute Difference, MRI vs CT	Correlation Coefficient, MRI vs CT
Flexion	122 ± 11 (98 to 141)	124 ± 12 (100 to 147)	3.5 ± 2.3 (0 to 9)	0.953
Extension	61 ± 32 (1 to 100)	63 ± 30 (0 to 100)	4.2 ± 3.0 (0 to 10)	0.987
Internal rotation in extension	114 ± 24 (84 to 169)	115 ± 21 (87 to 162)	4.4 ± 2.9 (0 to 10)	0.976
External rotation in extension	41 ± 22 (–3 to 82)	45 ± 21 (0 to 84)	3.8 ± 2.7 (0 to 10)	0.986
Abduction	61 ± 14 (22 to 82)	64 ± 14 (25 to 85)	4.2 ± 2.9 (0 to 10)	0.962
Adduction	29 ± 15 (1 to 56)	34 ± 15 (0 to 60)	5.1 ± 3.3 (0 to 11)	0.962
Internal rotation at 90° of flexion	36 ± 16 (9 to 67)	40 ± 16 (15 to 72)	5.2 ± 2.8 (0 to 10)	0.974
External rotation at 90° of flexion	99 ± 21 (32 to 125)	101 ± 21 (40 to 130)	4.0 ± 3.1 (0 to 10)	0.979

[a]Data are expressed as mean ± SD (range). 3D, 3-dimensional; CT, computed tomography; MRI, magnetic resonance imaging.
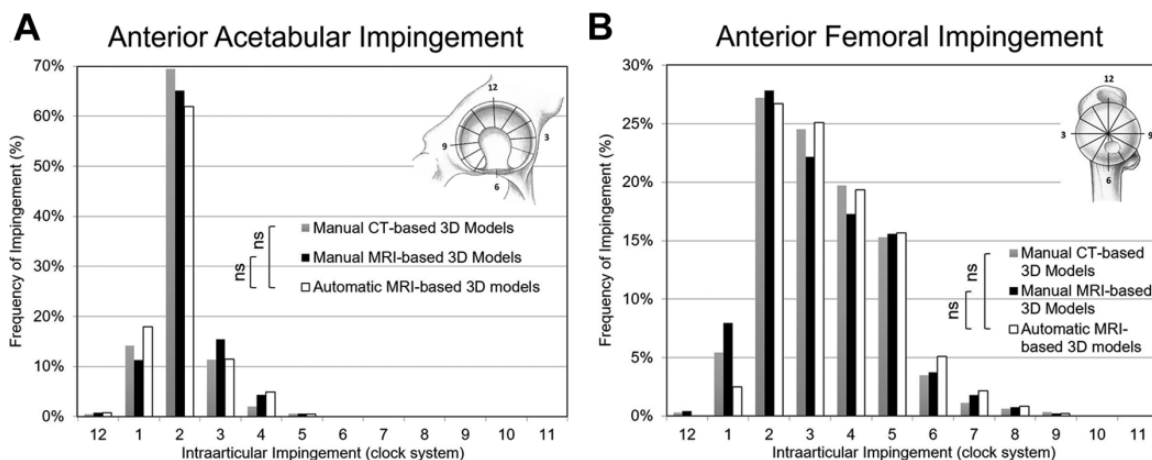
Figure 5. Results for the location of intra-articular (A) acetabular and (B) femoral impingement. ns, not significant.

The correlation of impingement-free flexion between CT-based and manual MRI-based 3D models was excellent ($r = 0.953$; $P < .001$) (Table 5). Correlation of impingement-free ROM was excellent and significant ($r = 0.994$; $P < .001$) between manual CT-based and automatic MRI-based 3D models (Figure 4D).

Location of Impingement

The location of intra-articular impingement was not significantly different between the manual and automatic MRI-based 3D models ($P = .758$), and the location of intra-articular acetabular and femoral impingement did

not differ between manual CT-based and automatic MRI-based 3D models ($P = .778$) (Figure 5). The location of extra-articular hip impingement was prevalent in 15 hips and did not differ between CT-based 3D models and MRI-based 3D models of the same 15 hips.

DISCUSSION

The aim of this study was to investigate the accuracy of these 2 methods when comparing impingement-free ROM and location of impingement. Matched CT-based and MRI-based 3D models of the same patients were compared. Most importantly, we found a high accuracy (Table 2) and an excellent correlation for ROM values between the manual and automatic MRI-based 3D models (Figure 4). Investigating location of impingement, we did not find a clinically relevant difference between the 2 methods (Figure 5). A novel finding of this study is that it used a fully automatic, radiation-free, patient-specific deep learning method for preoperative 3D impingement simulation. CNNs performed fast automatic bone segmentation of MRI-based 3D models with a duration of 1 to 5 minutes, while manual segmentation was very time-consuming (up to 4 hours). For future use of this technique, standardized MRI protocols could be important. Previous investigations for MRI-based 3D models of the hip joint and femur used other MRI protocols, performing manual segmentation and different methods for segmentation of the 3D models, that were not used for clinical routine application.[9,11] Various reasons, including small FOV, long AT, inhomogeneous bone intensity, or unclear boundaries between bone and the soft tissue, could possibly explain that.

Comparing the results of the accuracy of the 3D models, we found that previous studies reported a DSC of 84% to 86% upon comparing MRI segmentation for pediatric patients with hip dysplasia.[12] This is lower compared with our results (DSC, 97%-98%) (Table 2). A previous study investigating the accuracy of MRI-based 3D models reported a mean error of 0.23 mm for the segmentation of long bones. This is comparable with the results found for the ASD in our study (Table 2). Another study reported a higher ASD error, ranging from 0.55 to 0.75 mm, upon investigating automatic MRI segmentation of the femoral head and the acetabulum.[4] Two previous studies[9,10] reported an accuracy of 1.5 mm when investigating MRI segmentation with another method. Other studies only performed segmentation of the proximal femur[1] or did not report the DSC. This limits the comparison to the results found in the literature. Comparing manual CT segmentation with an automatic method, others have reported an ASD of 0.3 mm for the pelvis and the proximal femur.[5] This is a comparable value of the ASD compared with 0.2 ± 0.1 mm for femoral models and 0.3 ± 0.5 mm for acetabular models (Table 2) in our study. This difference found in our study is slightly lower compared with the previously reported manual segmentation[18] (range, 0.4-0.7 mm) but does not seem to be of clinical relevance.

We compared our results for impingement-free ROM (Table 4) with those of other studies. We found that our results are comparable with published ROM values for hips with anterior FAI and normal hip joints.[42] Another study found flexion to be $121° \pm 12°$ for normal hips and IR at $90°$ of flexion to be $35° \pm 12°$.[42] Previously, a lower flexion and IR at $90°$ of flexion were described for hips with anterior FAI.[42] This could be explained with the heterogeneity of the patients in this study (Table 1). We included hips with various hip deformities; 1 hip had a severe cam deformity (post-Perthes deformity). Therefore, the mean ROM values do not correspond to the published values for patients with FAI,[42] although we used the same software for the calculation of ROM values[27] (Table 5 and Figures 4 and 5). Another study described similar ROM values for flexion and for IR at $90°$ of flexion using a similar coordinate system.[25] Lower ROM values were described for patients with a prominent anterior-inferior iliac spine morphology.[13]

We analyzed our results for location of impingement and found that they compare well to the literature.[15,38,42] For example, for hips with anterior FAI with cam- or pincer-type morphologies, anterosuperior osseous impingement location[15,42] was reported. This is consistent with the results found in our study. An advantage is that the acetabular and femoral impingement location detected during the 2 clinically used motion patterns (anterior and posterior impingement test) can be directly translated to the clinical examination.

This study aimed to compare CT-based and MRI-based 3D models (see Video Supplements 1 and 2) of the hip joint of the same patients. Previous studies compared the segmentation results or the CT-based or MRI-based segmentation of 3D models in cadavers[28,47] or animal models[47] or with different methods for segmentation.[2,6] Another strength of this study is that this method could be used for detailed localization of impingement, including intra- and extra-articular FAI (Figure 4). Information about extra-articular FAI is very important in patients with abnormal FV[17] and for patients with pincer-type FAI.[20] In addition, detailed 3D information of the acetabulum is essential for the decision making for surgical therapy in hips with pincer-type FAI.[36] Important ROM values for anterior FAI include flexion and IR at $90°$ of flexion. For both flexion ($r = 0.953$; $P < .001$) and IR at $90°$ of flexion ($r = 0.982$; $P < .001$) (Table 4), a good correlation between automatic and manual MRI-based 3D models (Figure 4) and between CT-based and MRI-based 3D models (Table 5) was achieved.

This study has limitations. First, we exclusively included hips without previous operations and with complete MRI and CT data sets. Hips with previous operations often had MRI artifacts, and we were unable to perform accurate MRI segmentation in them. Second, we included only hips without osteoarthritis (Tönnis grade >2). This was necessary because the patients eligible for joint-preserving hip surgery are often young and have no osteoarthritis. Third, we had a small number of patients in general and especially with severe deformities such as avascular necrosis of the femoral head (2 hips; 6%). This is because of the study

design with consecutive analysis of patients and because protrusio acetabuli is a rare hip morphology. This could also be a strength because it showed that the applied method was applicable for severe hip deformities too. In addition, the time-consuming manual segmentation included manual steps that are potential sources of error and inter- and intraobserver variability. To avoid this, we performed 30 manual segmentations of MRI-based 3D models for training, which are not included in the current study. Another limitation of bone segmentation is the lack of soft tissue, such as the capsule or acetabular labrum. This could influence hip ROM as well and could be one of the reasons for the moderate correlation coefficient between clinical and simulated ROMs for ER at 90° of flexion and for flexion (Supplemental Table S4 and Figure S4). The largest correlation coefficient between clinical ROM and simulated ROM was found for IR at 90° of flexion (Supplemental Table S4 and Figure S4), and this parameter was considered the most important parameter for surgical planning for patients with FAI.

This study has clinical implications. Impingement simulation allows patient-specific detection of FAI, especially extra-articular hip impingement. This could be applied to all patients undergoing MRI for screening for extra-articular hip impingement before hip arthroscopy. Patient-specific impingement simulation could be helpful to plan cam resection for patients with extra-articular hip impingement. Whether femoral cam resection can restore normal ROM in patients with extra-articular hip impingement should be evaluated in the future. Treatment of hips with extra-articular hip impingement and decreased FV is controversial; some authors have reported that the amount of FV does not affect the clinical outcomes after treatment with hip arthroscopy.[14] Some other surgeons have described decreased FV as a relative contraindication to corrective FAI surgery,[25,46] as it has been found to be a risk factor for inferior outcomes after treatment with hip arthroscopy.[7]

Based on the results found in our study, we will change our clinical practice and use automatic MRI-based 3D models instead of CT-based 3D models for preoperative calculation of impingement-free ROM. In addition, they could be used for radiation-free surgical planning of hip arthroscopy or femoral derotation osteotomy.[19] Automatic segmentation of MRI-based 3D models can potentially reduce the need for preoperative pelvic CT scans in young patients with hip pain. Furthermore, MRI-based 3D models allow the analysis of impingement-free ROM and detection of FAI in pediatric patients, such as pediatric patients with slipped capital femoral epiphysis,[23,41,51] Legg-Calvé-Perthes disease,[39] and hip dysplasia.[21] Standardized MRI protocols are important for future use of this technique.

We found high accuracy for the 3D MRI bone models of the hip joint in this study. In addition, we found high accuracy for impingement-free hip ROM and location of impingement using the created 3D models with the help of deep learning (CNN) compared with manual segmentation. The location of hip impingement was not different between CT- and MRI-based 3D models.

CONCLUSION

CNN can potentially be used in clinical practice to provide rapid and accurate 3D MRI hip joint models for young patients. Created models can be used for simulation of hip impingement for diagnosis of intra- and extra-articular hip impingement for radiation-free and patient-specific preoperative surgical planning for hip arthroscopy and open hip preservation surgery. We recommend using standardized MRI protocols for future use of this technique.

A Video Supplement for this article is available at http://journals.sagepub.com/doi/suppl/10.1177/23259671211046916.

REFERENCES

1. Arezoomand S, Lee WS, Rakhra KS, Beaulé PE. A 3D active model framework for segmentation of proximal femur in MR images. *Int J Comput Assist Radiol Surg*. 2015;10(1):55-66. doi:10.1007/s11548-014-1125-6
2. Blum S, Franken L, Hartmann A, et al. MRI-based static and functional assessment of complex hip deformities in comparison with CT: a validation study. *MAGMA*. 2020;33(6):829-838. doi:10.1007/s10334-020-00845-5
3. Casartelli NC, Brunner R, Maffiuletti NA, et al. The FADIR test accuracy for screening cam and pincer morphology in youth ice hockey players. *J Sci Med Sport*. 2018;21(2):134-138. doi:10.1016/j.jsams.2017.06.011
4. Chandra SS, Xia Y, Engstrom C, Crozier S, Schwarz R, Fripp J. Focused shape models for hip joint segmentation in 3D magnetic resonance images. *Med Image Anal*. 2014;18(3):567-578. doi:10.1016/j.media.2014.02.002
5. Chu C, Bai J, Wu X, Zheng G. MASCG: Multi-Atlas Segmentation Constrained Graph method for accurate segmentation of hip CT images. *Med Image Anal*. 2015;26(1):173-184. doi:10.1016/j.media.2015.08.011
6. Damopoulos D, Lerch TD, Schmaranzer F, et al. Segmentation of the proximal femur in radial MR scans using a random forest classifier and deformable model registration. *Int J Comput Assist Radiol Surg*. 2019;14(3):545-561. doi:10.1007/s11548-018-1899-z
7. Fabricant PD, Fields KG, Taylor SA, Magennis E, Bedi A, Kelly BT. The effect of femoral and acetabular version on clinical outcomes after arthroscopic femoroacetabular impingement surgery. *J Bone Joint Surg Am*. 2015;97(7):537-543. doi:10.2106/JBJS.N.00266
8. Ganz R, Parvizi J, Beck M, Leunig M, Nötzli H, Siebenrock KA. Femoroacetabular impingement: a cause for osteoarthritis of the hip. *Clin Orthop Relat Res*. 2003;417:112-120. doi:10.1097/01.blo.0000096804.78689.c2
9. Gilles B, Magnenat-Thalmann N. Musculoskeletal MRI segmentation using multi-resolution simplex meshes with medial representations. *Med Image Anal*. 2010;14(3):291-302. doi:10.1016/j.media.2010.01.006
10. Gilles B, Moccozet L, Magnenat-Thalmann N. Anatomical modelling of the musculoskeletal system from MRI. *Med Image Comput Comput Assist Interv*. 2006;9(pt 1):289-296. doi:10.1007/11866565_36
11. Gilles B, Perrin R, Magnenat-Thalmann N, Vallee JP. Bone motion analysis from dynamic MRI: acquisition and tracking. *Acad Radiol*. 2005;12(10):1285-1292. doi:10.1016/j.acra.2005.08.006
12. Hareendranathan AR, Zonoobi D, Mabee M, et al. Hip segmentation from MRI volumes in infants for DDH diagnosis and treatment planning. *Conf Proc IEEE Eng Med Biol Soc*. 2016;2016:1046-1049. doi:10.1109/EMBC.2016.7590882

13. Hetsroni I, Poultsides L, Bedi A, Larson CM, Kelly BT. Anterior inferior iliac spine morphology correlates with hip range of motion: a classification system and dynamic model. *Clin Orthop Relat Res*. 2013;471(8):2497-2503. doi:10.1007/s11999-013-2847-4

14. Jackson TJ, Lindner D, El-Bitar YF, Domb BG. Effect of femoral anteversion on clinical outcomes after hip arthroscopy. *Arthroscopy*. 2015;31(1):35-41. doi:10.1016/j.arthro.2014.07.009

15. Kubiak-Langer M, Tannast M, Murphy SB, Siebenrock KA, Langlotz F. Range of motion in anterior femoroacetabular impingement. *Clin Orthop Relat Res*. 2007;458:117-124. doi:10.1097/BLO.0b013e318031c595

16. Lall AC, Battaglia MR, Maldonado DR, et al. Does femoral retroversion adversely affect outcomes after hip arthroscopy for femoroacetabular impingement syndrome? A midterm analysis. *Arthroscopy*. 2019;35(11):3035-3046. doi:10.1016/j.arthro.2019.03.046

17. Lerch TD, Boschung A, Todorski IAS, et al. Femoroacetabular impingement patients with decreased femoral version have different impingement locations and intra- and extraarticular anterior subspine FAI on 3D-CT-based impingement simulation: implications for hip arthroscopy. *Am J Sports Med*. 2019;47(13):3120-3132. doi:10.1177/0363546519873666

18. Lerch TD, Degonda C, Schmaranzer F, et al. Patient-specific 3-D magnetic resonance imaging-based dynamic simulation of hip impingement and range of motion can replace 3-D computed tomography-based simulation for patients with femoroacetabular impingement: implications for planning open hip preservation surgery and hip arthroscopy. *Am J Sports Med*. 2019;47(12):2966-2977. doi:10.1177/0363546519869681

19. Lerch TD, Schmaranzer F, Steppacher SD, Ziebarth K, Tannast M, Siebenrock KA. Most of patients with femoral derotation osteotomy for posterior extraarticular hip impingement and high femoral version would do surgery again. *Hip Int*. Published online August 31, 2020. doi:10.1177/1120700020953100

20. Lerch TD, Siegfried M, Schmaranzer F, et al. Location of intra- and extra-articular hip impingement is different in patients with pincer-type and mixed-type femoroacetabular impingement due to acetabular retroversion or protrusio acetabuli on 3D CT-based impingement simulation. *Am J Sports Med*. 2020;48(3):661-672. doi:10.1177/0363546519897273

21. Lerch TD, Steppacher SD, Liechti EF, Tannast M, Siebenrock KA. One-third of hips after periacetabular osteotomy survive 30 years with good clinical results, no progression of arthritis, or conversion to THA. *Clin Orthop Relat Res*. 2017;475(4):1154-1168. doi:10.1007/s11999-016-5169-5

22. Lerch TD, Todorski IAS, Steppacher SD, et al. Prevalence of femoral and acetabular version abnormalities in patients with symptomatic hip disease: a controlled study of 538 hips. *Am J Sports Med*. 2018;46(1):122-134. doi:10.1177/0363546517726983

23. Lerch TD, Vuilleumier S, Schmaranzer F, et al. Patients with severe slipped capital femoral epiphysis treated by the modified Dunn procedure have low rates of avascular necrosis, good outcomes, and little osteoarthritis at long-term follow-up. *Bone Joint J*. 2019;101(4):403-414. doi:10.1302/0301-620X.101B4.BJJ-2018-1303.R1

24. Lerch TD, Zwingelstein S, Schmaranzer F, et al. Posterior extra-articular ischiofemoral impingement can be caused by the lesser and greater trochanter in patients with increased femoral version: dynamic 3D CT-based hip impingement simulation of a modified FABER test. *Orthop J Sports Med*. 2021;9(5):2325967121990629. doi:10.1177/2325967121990629

25. Nakahara I, Takao M, Sakai T, Nishii T, Yoshikawa H, Sugano N. Gender differences in 3D morphology and bony impingement of human hips. *J Orthop Res*. 2011;29(3):333-339. doi:10.1002/jor.21265

26. Pfirrmann CWA, Sutter R. Hip imaging. *Semin Musculoskelet Radiol*. 2017;21(5):485-486. doi:10.1055/s-0037-1606142

27. Puls M, Ecker TM, Tannast M, Steppacher SD, Siebenrock KA, Kowal JH. The equidistant method—a novel hip joint simulation algorithm for detection of femoroacetabular impingement. *Comput Aided Surg*. 2010;15(4-6):75-82. doi:10.3109/10929088.2010.530076

28. Rathnayaka K, Momot KI, Noser H, et al. Quantification of the accuracy of MRI generated 3D models of long bones compared to CT generated 3D models. *Med Eng Phys*. 2012;34(3):357-363. doi:10.1016/j.medengphy.2011.07.027

29. Reiman MP, Goode AP, Cook CE, Hölmich P, Thorborg K. Diagnostic accuracy of clinical tests for the diagnosis of hip femoroacetabular impingement/labral tear: a systematic review with meta-analysis. *Br J Sports Med*. 2015;49(12):811. doi:10.1136/bjsports-2014-094302

30. Ricciardi BF, Fabricant PD, Fields KG, Poultsides L, Zaltz I, Sink EL. What are the demographic and radiographic characteristics of patients with symptomatic extraarticular femoroacetabular impingement? *Clin Orthop Relat Res*. 2015;473(4):1299-1308. doi:10.1007/s11999-014-4001-3

31. Schmaranzer F, Hanke M, Lerch T, Steppacher S, Siebenrock K, Tannast M. Impingement of the hip. Article in German. *Radiologe*. 2016;56(9):825-838. doi:10.1007/s00117-016-0136-4

32. Schmaranzer F, Klauser A, Kogler M, et al. Diagnostic performance of direct traction MR arthrography of the hip: detection of chondral and labral lesions with arthroscopic comparison. *Eur Radiol*. 2015;25(6):1721-1730. doi:10.1007/s00330-014-3534-x

33. Schmaranzer F, Lerch TD, Siebenrock KA, Tannast M, Steppacher SD. Differences in femoral torsion among various measurement methods increase in hips with excessive femoral torsion. *Clin Orthop Relat Res*. 2019;477(5):1073-1083. doi:10.1097/CORR.0000000000000610

34. Schmaranzer F, Lerch TD, Strasser U, Vavron P, Schmaranzer E, Tannast M. Usefulness of MR arthrography of the hip with and without leg traction in detection of intra-articular bodies. *Acad Radiol*. 2019;26(9):e252-e259. doi:10.1016/j.acra.2018.10.008

35. Siebenrock KA, Steppacher SD, Haefeli PC, Schwab JM, Tannast M. Valgus hip with high antetorsion causes pain through posterior extra-articular FAI. *Clin Orthop Relat Res*. 2013;471(12):3774-3780. doi:10.1007/s11999-013-2895-9

36. Steppacher SD, Lerch TD, Gharanizadeh K, et al. Size and shape of the lunate surface in different types of pincer impingement: theoretical implications for surgical therapy. *Osteoarthritis Cartilage*. 2014;22(7):951-958. doi:10.1016/j.joca.2014.05.010

37. Sutter R, Dietrich TJ, Zingg PO, Pfirrmann CWA. How useful is the alpha angle for discriminating between symptomatic patients with cam-type femoroacetabular impingement and asymptomatic volunteers? *Radiology*. 2012;264(2):514-521. doi:10.1148/radiol.12112479

38. Tannast M, Goricki D, Beck M, Murphy SB, Siebenrock KA. Hip damage occurs at the zone of femoroacetabular impingement. *Clin Orthop Relat Res*. 2008;466(2):273-280. doi:10.1007/s11999-007-0061-y

39. Tannast M, Hanke M, Ecker TM, Murphy SB, Albers CE, Puls M. LCPD: reduced range of motion resulting from extra- and intraarticular impingement. *Clin Orthop Relat Res*. 2012;470(9):2431-2440. doi:10.1007/s11999-012-2344-1

40. Tannast M, Hanke MS, Zheng G, Steppacher SD, Siebenrock KA. What are the radiographic reference values for acetabular under- and overcoverage? *Clin Orthop Relat Res*. 2015;473(4):1234-1246. doi:10.1007/s11999-014-4038-3

41. Tannast M, Jost LM, Lerch TD, Schmaranzer F, Ziebarth K, Siebenrock KA. The modified Dunn procedure for slipped capital femoral epiphysis: the Bernese experience. *J Child Orthop*. 2017;11(2):138-146. doi:10.1302/1863-2548-11-170046

42. Tannast M, Kubiak-Langer M, Langlotz F, Puls M, Murphy SB, Siebenrock KA. Noninvasive three-dimensional assessment of femoroacetabular impingement. *J Orthop Res*. 2007;25(1):122-131. doi:10.1002/jor.20309

43. Tannast M, Mistry S, Steppacher SD, et al. Radiographic analysis of femoroacetabular impingement with Hip2Norm—reliable and validated. *J Orthop Res*. 2008;26(9):1199-1205. doi:10.1002/jor.20653

44. Tannast M, Siebenrock KA, Anderson SE. Femoroacetabular impingement: radiographic diagnosis—what the radiologist should know. *AJR Am J Roentgenol*. 2007;188(6):1540-1552. doi:10.2214/AJR.06.0921

45. Tong KM, Lee TS, Lin YM, Pfirrmann CWA. Cam and pincer impingements rarely occur in isolation. *Radiology*. 2007;244(2):625-626. doi:10.1148/radiol.2442061498

46. Tönnis D, Heinecke A. Acetabular and femoral anteversion: relationship with osteoarthritis of the hip. *J Bone Joint Surg Am*. 1999;81(12):1747-1770.

47. Van den Broeck J, Vereecke E, Wirix-Speetjens R, Vander Sloten J. Segmentation accuracy of long bones. *Med Eng Phys*. 2014;36(7):949-953. doi:10.1016/j.medengphy.2014.03.016

48. Wylie JD, Jenkins PA, Beckmann JT, Peters CL, Aoki SK, Maak TG. Computed tomography scans in patients with young adult hip pain carry a lifetime risk of malignancy. *Arthroscopy*. 2018;34(1):155-163.e3. doi:10.1016/j.arthro.2017.08.235

49. Zeng G, Zheng G. Holistic decomposition convolution for effective semantic segmentation of medical volume images. *Med Image Anal*. 2019;57:149-164. doi:10.1016/j.media.2019.07.003

50. Zheng G, Tannast M, Anderegg C, Siebenrock KA, Langlotz F. Hip2Norm: an object-oriented cross-platform program for 3D analysis of hip joint morphology using 2D pelvic radiographs. *Comput Methods Programs Biomed*. 2007;87(1):36-45. doi:10.1016/j.cmpb.2007.02.010

51. Ziebarth K, Milosevic M, Lerch TD, Steppacher SD, Slongo T, Siebenrock KA. High survivorship and little osteoarthritis at 10-year followup in SCFE patients treated with a modified Dunn procedure. *Clin Orthop Relat Res*. 2017;475(4):1212-1228. doi:10.1007/s11999-017-5252-6